Structural Characterization of Polyetherimide-Based Carbon Molecular Sieve Membranes

Mehran G. Sedigh, Maryam Jahangiri, Paul K. T. Liu, Muhammad Sahimi, and Theodore T. Tsotsis
Dept. of Chemical Engineering, University of Southern California, Los Angeles, CA 90089

Supported carbon molecular sieve membranes (CMSMs) were prepared by the pyrolysis of a polyetherimide (PEI) polymeric precursor. The membranes were characterized by scanning electron microscopy, energy dispersive spectroscopy, and micropore analysis, using gas adsorption techniques to relate their microstructure characteristics to their transport and separation characteristics. The analysis shows that preparation conditions determine whether the carbon molecular sieve layer forms within or outside the γ-alumina layer of the substrate. Micropore CO_2 and N_2 adsorption analysis of both supported and unsupported CMSMs showed a sharp peak at about $(3.6-3.8)\times 10^{-10}$ m using the Horvath-Kawazoe method. For the supported CMSMs it was observed that consecutive coating/carbonization steps reduced the pore volume in the micro- and mesoporous regions, without greatly affecting the volume of pores in the range of $(3.5-6)\times 10^{-10}$ m. The reduction of the pore volume in the micro- and mesoporous regions is accompanied by an increase in the separation factor and a decrease in the permeance after each coating/carbonization cycle. Micropore analysis of a membrane, whose performance had degraded, indicated that its volume of pores between $(3.6-6)\times 10^{-10}$ m had drastically decreased from the corresponding value of the as-prepared membranes.

Introduction

The use of carbon molecular sieve membranes (CMSMs) has been studied in the last few years as a promising alternative technology to more energy-demanding conventional processes for gas separation applications. A potential such application involves separation of an adsorptive component such as CO_2 or a light hydrocarbon (C_2—C_4) from its mixture with less adsorptive components at low to moderate temperatures and feed pressures. CMSMs are prepared either through the carbonization of preexisting polymeric substrates (such as hollow fibers, or self-supporting thin films) or through the carbonization of films deposited on underlying macro- and mesoporous supports by pyrolysis, typically in an inert atmosphere. The pyrolysis is carried out at temperatures ranging from 773 K to 1,273 K. Depending on the conditions, the pyrolysis process removes part of the heteroatoms, originally present in the polymer structure, while leaving behind a cross-linked and stiff, mostly carbon matrix. The CMSMs so prepared have an amorphous microporous structure created by the evolution of gases as a result of the rearrangement of the molecular structure of the starting polymeric precursor during the pyrolysis process.

Of importance for membranes, including CMSMs, are their transport and separation characteristics. These characteristics, typically studied by transport experiments, not only reveal the potential of these membranes for a range of separation applications, but also provide a better understanding of the permeation and separation mechanisms in a given membrane under various operating conditions. In the last few years several groups, including ours (Sedigh et al., 1998, 1999), have studied the transport and separation characteristics of different types of supported or unsupported CMSMs for several gaseous mixtures (for a brief review of the results of these studies see, for example, Sedigh et al., 1999). The motivation behind all these studies is to optimize the membrane preparation process, to develop membranes with a higher separa-

Correspondence concerning this article should be addressed to T. T. Tsotsis.
Present addresses of: M. G. Sedigh, Cypress Semiconductor, Research and Development Div., 3901 North First St., San Jose, CA 95134; P. K. T. Liu, Media and Process Technology, Inc., 1155 William Pitt Way, Pittsburgh, PA 15238.

tion factor and permeance, better operability and stability, and less of a production cost. To accomplish this goal it is important to be able to relate the transport and separation characteristics of these membranes to their structural characteristics. This involves knowing the structural and transport characteristics of these membranes as they go through the different stages of preparation. Such an understanding is the key to achieving a reliable optimized preparation technique and more reproducible results.

Several experimental techniques have been used through the years in order to gain a better understanding of the structure of the CMSMs. Different types of electron microscopy, including scanning electron microscopy (SEM) and transmission electron microscopy (TEM), are among the most common techniques. They have been utilized to provide a picture of the cross section as well as of the surface texture of both supported and unsupported CMSMs (Rao and Sircar, 1993; Limkov et al., 1994a,b; Chen and Yang, 1994; Hayashi et al., 1995, 1996, 1997; Acharya et al., 1997; Steriotis et al., 1997; Sedigh et al., 1999). These techniques are useful to some extent, in evaluating the overall quality of the selective layer, the presence of any macro-/mesoscopic cracks or pinholes, and for determining the apparent thickness of the permselective layer. However, electron microscopy techniques, due to the limitation of the electron beam width, cannot probe feature sizes in the microporous range. They are therefore unable to provide meaningful information regarding the pore-size characteristics of the microporous permselective carbon layer.

In recent years advances in scanned probe microscopy techniques, such as scanning tunneling microscopy (STM) and atomic-force microscopy (AFM), have made it possible to look at the surface of microporous materials in greater detail than it was ever possible before using electron microscopy techniques (Hoffman et al., 1994; Economy et al., 1995; Rao and Sircar, 1996). These techniques certainly provide a better understanding of surface roughness and texture. However, scanned probe microscopy techniques have their own shortcomings. Notable among them is the sensitivity of the probe to surface roughness. Since the probe tip has a certain size (a few angstroms typically), it does not penetrate into openings (pores) that are smaller than its size. It therefore does not probe the microscopic details of the surface. In addition, scanned probe microscopy techniques are known to create image artifacts. Both electron and probe microscopy techniques have the distinct disadvantage of being local techniques, and thus not providing overall properties and characteristics of microporous materials.

In addition to microscopy techniques, there is another group of techniques available for structural characterization of microporous materials. These techniques are based on adsorption or condensation of different types of probe molecules within the material's porous structure at a specified pressure and temperature. Adsorption-based techniques have been widely used for obtaining the surface area, pore volume, mean pore-size, and pore-size distribution of many different microporous materials, including activated carbons (Inagaki and Nakashima, 1992; Ehrburger et al., 1992; Miura et al., 1993; Koresh, 1993; Kumita et al., 1995; Setoyama et al., 1996; Yoshizawa et al., 1996), and carbon molecular sieves (CMS) (Miura et al., 1993; Jagiello et al., 1995; Nakashima et al., 1995; Steriotis et al., 1997). The main advantage of these techniques is that, unlike the microscopy techniques, they are not local techniques capable only of probing a thin layer near the surface. Instead, they are capable of generating overall characterization data for the microporous materials of interest. These data can then be used for generating a complete picture of the pore network in terms of its pore volume, surface area, and pore-size distribution. The adsorption-based techniques are, however, limited in the resolution of the pore sizes by the size of the probe molecules that are accessible into the pore structure. For most membrane applications, however, this does not present a limitation. The main disadvantage of the adsorption-based techniques is in choosing the appropriate pore model for the interpretation of the adsorption data. Since one does not have *a priori* knowledge of the pore structure, this makes it difficult to estimate the absolute size parameters.

From the preceding discussion it should be clear that microscopy and adsorption techniques have their own individual limitations. Applied in combination, however, they provide the best available tools for the characterization of microporous materials. We have applied both techniques for the structural characterization of the CMSMs that have been prepared by our group (Sedigh et al., 1999). These are prepared by the pyrolysis of polyetherimide (PEI) polymeric precursors supported on meso-/macroporous supports. The objective of the study was to obtain a better picture of the structure of these membranes, and to create a connection between the structure and the membrane's separation and transport characteristics.

Experimental Techniques

Membrane preparation

To prepare the supported CMSMs from PEI precursors, support substrates consisting of cylindrical ceramic tubes (0.007 m ID, 0.010 m OD, and 0.045 m long), manufactured by U.S. Filter, were dip-coated in a PEI solution. These support tubes have a thin layer of γ-alumina, with an average pore diameter of 5×10^{-9} m on the inside of the tube (Sedigh et al., 1998). The average argon permeance, which was used as a yard stick for appropriateness of substrates, was in the range of $[3.481\times10^{-6}-3.481\times10^{-5}]$ $m^3/m^2\cdot Pa\cdot s$. To prepare the PEI solution with proper concentration, Ultem 1000 (supplied by GE) was dissolved in 1,2 dichloroethane (DCE). As is explained later in the following discussion, the concentration of the polymeric precursor solution has a significant effect on where the selective carbogenic layer forms, and on its characteristics. Therefore, for the preparation of the CMSM it is important to select the polymeric precursor solution with the appropriate concentration. Unless otherwise noted, for all the membranes referred to in this article a 6 wt. % PEI/DCE solution was used for coating the initial substrate, and a 2% solution was used for all the following coating stages. After coating, the membrane was dried in air for one day, and was then tested with He and N_2/Ar to make sure that the layer is free of any cracks and pinholes. Details of the coating method and preliminary tests were described in detail elsewhere (Sedigh et al., 1999).

After coating with the PEI film, the membrane was carbonized in the presence of flowing Ar (99.997% pure) in a

cylindrical furnace, 0.0508 m diameter and 0.6096 m long, externally heated and controlled by a programmable Omega CN3000 controller. The membrane was placed between two thermocouples about 0.05 m apart with the tip of the thermocouples close to the outside surface of the membrane to make sure that no temperature gradient exists along the axis of the membrane. An Ar flow rate of $(1-1.33)\times 10^{-6}$ m^3/s was used to remove the gases evolved during carbonization and to maintain the inert atmosphere.

The carbonization protocol involved raising the temperature slowly (0.0167 K/s)—to prevent crack formation during carbonization—and holding it constant first at 623 K for 1,800 s, and then at 873 K for 14,400 s. Subsequently, the membrane was cooled to 453 K at a rate of 0.0333 K/s, and to room temperature at a rate of 0.0833 K/s. The coating/carbonization procedure was repeated as many times as required to modify the selective layer, in order to achieve the desired membrane separation factor and permeance. We have also prepared unsupported pyrolyzed PEI samples. These were prepared according to the same carbonization procedure by placing a weighed amount of PEI in a Coors ceramic crucible in between the thermocouples inside the furnace.

Membrane characterization

The permeation of single gases (CH_4, CO_2, Ar, and H_2) and mixtures of the same gases through the carbonized membrane was measured after each carbonization step, in order to evaluate the membrane's transport characteristics. Details of the transport characterization system and the experimental techniques we followed are described elsewhere (Sedigh et al., 1999).

SEM and EDS studies were performed at the Center for Electron Microscopy and Microanalysis (CEMMA) of the University of Southern California, using a Cambridge 360 SEM instrument (Cambridge Instruments, UK). The nonconductive samples, that is, alumina and polymer-coated supports, were prepared for SEM by gold deposition on the surface using a DC sputtering technique at 53320 Pa with an Ar plasma. Supported CMSMs were studied without any gold sputtering due to their semiconductive carbon layer. For the EDS studies of the polymer-coated substrates, however, the surface was sputtered with high-purity graphite to prevent the interference of the gold peak that could have been caused by gold sputtering.

Gas adsorption experiments were performed in a static mode using an ASAP 2010 micropore analyzer from Micromeritics, Inc., Norcross, GA. The system was equipped with a turbomolecular pump that was able to create a vacuum down to 1.33×10^{-3} Pa. A special analysis port together with a bigger-diameter sample tube were designed and built. This enabled us to measure the pore volume, surface area, and pore-size distribution of the membranes after each carbonization or degradation step, without the need to crushing them in order to place them in the standard sample tube. Incremental volume dosing instead of the pressure table, which measures the gas uptake within a certain interval close to a prespecified relative pressure, was followed in the low relative pressure region, that is, for less than 0.1. This is in order to ensure the accuracy of the measured pore-size distribution in that region of the isotherms. The desired dosing volume is usually obtained by a preliminary run to measure total pore volume at a relative pressure of 0.1. The dosing volume was found by dividing the measured pore volume by the total number of points required in that region of the isotherm. Following this method the sample is dosed by a certain amount of gas in each step, which therefore generates a more accurate pore-size distribution in the low-pressure region, where all the micropores are found. The samples were degassed on the analysis port (after being partially degassed on the degassing port) to take advantage of the ultrahigh vacuum created by the molecular drag pump. The degassing of the CMSM usually took about 2 days at 473–513 K, while it took about 3 days to degas the pyrolyzed powder, due to the very microporous nature of the powder and the diffusion limitation of the desorbed gases through the tight pore network of the powder. Moreover, to eliminate the problems that might be caused by helium entrapment inside the micropores during free-space measurements, the tests were always stopped after the free-space measurement, and the samples were degassed under the same conditions for as long as it was required. The second degassing step took approximately 1 to 2 days for the supported CMSMs and CMS prepared by pyrolysis of PEI.

The N_2 adsorption tests were performed at 77 K, and an isothermal jacket around the sample tube maintained the level of liquid nitrogen constant for up to one day. For longer runs, which was normally the case for CMSMs and CMS, both the sample Dewar and the cold trap Dewar needed to be refilled. In this case the system was stopped for about one hour in order to establish equilibrium before resuming the run. The CO_2 adsorption tests were performed at 273 K using an ice-water isothermal bath. Compared to the liquid nitrogen temperature, this high temperature greatly enhanced the diffusion process through the pore network and shortened the duration of the analysis. However, due to the very high vapor pressure of CO_2 at 273 K, (3.481×10^6 Pa), and the physical limitations of the system (maximum pressure of 1.233×10^5 Pa), we were unable to extend the CO_2 analysis beyond a relative pressure of 0.03. According to the HK model used in our calculations, this relative pressure corresponds to pore widths of up to 6×10^{-10} m. Therefore, despite its associated difficulties and long run duration, the N_2 adsorption test was utilized in routine applications in order to obtain the overall PSD both in the micro- and mesoporous regions.

Results and Discussion

Scanning electron microscopy and energy dispersive spectroscopy

In order to understand the effect of the coating/carbonization cycle on the substrate and to find out where the selective carbon film is formed and how it modifies the underlying support structure, the cross section of the membrane at different stages of the coating/carbonization cycle were studied by electron microscopy. As noted previously, for most of the samples investigated the first coating utilized a 6% PEI in DCE solution. For subsequent coatings (after the first coating had been carbonized) we utilized a 2% PEI/DCE solution. The concentrations of the polymeric precursor solutions and the carbonization procedures followed are the same as those used for the membranes prepared for the transport and

separation, and gas adsorption characterization experiments. For a number of membranes we also performed the first coating using PEI solutions of a higher concentration. The goal for these experiments was to identify conditions for which the polymeric film will mostly form inside or outside the topmost support substrate layer.

Figure 1a is a low-magnification (1K) SEM picture of a cross section of the original alumina substrate after it had been gold-sputtered. There are four distinct regions in this SEM image. The bottom part, with a coarse, granular structure, is the macroporous α-alumina layer, with a reported (by the manufacturer) average pore diameter of about 1.5×10^{-5} m. This layer, which is about 1.5×10^{-3} m thick, provides the mechanical strength for the alumina membrane. It is covered by two other α-alumina layers that appear to have finer granular structures, with reported (by the manufacturer) average pore diameters of 8×10^{-7} m and 2×10^{-7} m, respectively. In Figure 1a, one observes a thin layer on top of these two layers, with an average thickness of $(2-3)\times10^{-6}$ m. This layer,

Figure 1. SEM images of the cross section of the alumina substrate: (a) 1 K magnification; (b) 10 K magnification.

Figure 2. SEM image of the cross section of the polymer coated substrate: (a) 1 K magnification; (b) 10 K magnification.

which at this SEM resolution looks smooth and nonporous, is the γ-alumina layer which, according to the manufacturer, has an average pore diameter of 5×10^{-9} m. Figure 1b is a higher-magnification (10K) picture of the same membrane cross section. Although gold-sputtering tends to smooth out surface features, it is still possible to recognize that the γ-alumina layer is indeed porous.

Figures 2a and 2b show the cross section of the membrane after it had been dip-coated once in a 6 wt. % PEI in DCE solution at 1K and 10K magnification, respectively. It can be observed in Figure 2a that the polymer solution has penetrated beyond the inner γ-alumina layer and into the underlying 2×10^{-7}-m and 8×10^{-7}-m average pores-size α-alumina layers. Comparing Figure 1a with Figures 2a and 2b, it is clear that as a result of the dip-coating process, the void volume in the γ-alumina layer is filled with the polymer. Moreover, it can be seen from Figure 2b (within the resolution in this SEM picture) for the sample dip-coated with the 6% solution there is no distinct polymer film on the top of the substrate.

Whether the polymeric film completely penetrates the underlying γ-alumina layer or mostly stays on the top depends on the concentration of the polymeric solution and the conditions of dip-coating (and, of course, the nature of the underlying substrate—however, this goes beyond the scope of this article). To investigate this issue we have found it helpful to couple electron microscopy with EDS.

In order to verify the effect that the concentration of the polymeric solution has on the position of the polymeric layer, we have coated a number of U.S. Filter tubes with polymeric solutions of varying concentration. To investigate the effect of concentration alone we have kept the other dip-coating conditions constant. The membranes were left in the solution for 180 s, after which time they were pulled out at a constant rate of 2×10^{-4} m/s. After being dried for 2 days, all the membranes were sputtered with high-purity graphite. Replacing gold with graphite removes possible interference from the gold peak in the EDS spectra, and at the same time creates a conductive surface, which is required for electron spectroscopy.

Figure 3 shows the EDS results obtained by scanning a $1.5\times10^{-5}\times1.5\times10^{-5}$ m^2 surface of three different samples prepared by the procedure described earlier using 6 wt. %, 10 wt. % and 15 wt. % PEI in DCE solutions. The analysis in Figure 3 was done using an electron beam generated by a 10-kV accelerating voltage. There is a distinct Al peak, representing the γ-alumina substrate, for the sample that was coated with the 6 wt. % solution (Figure 3a). There are no

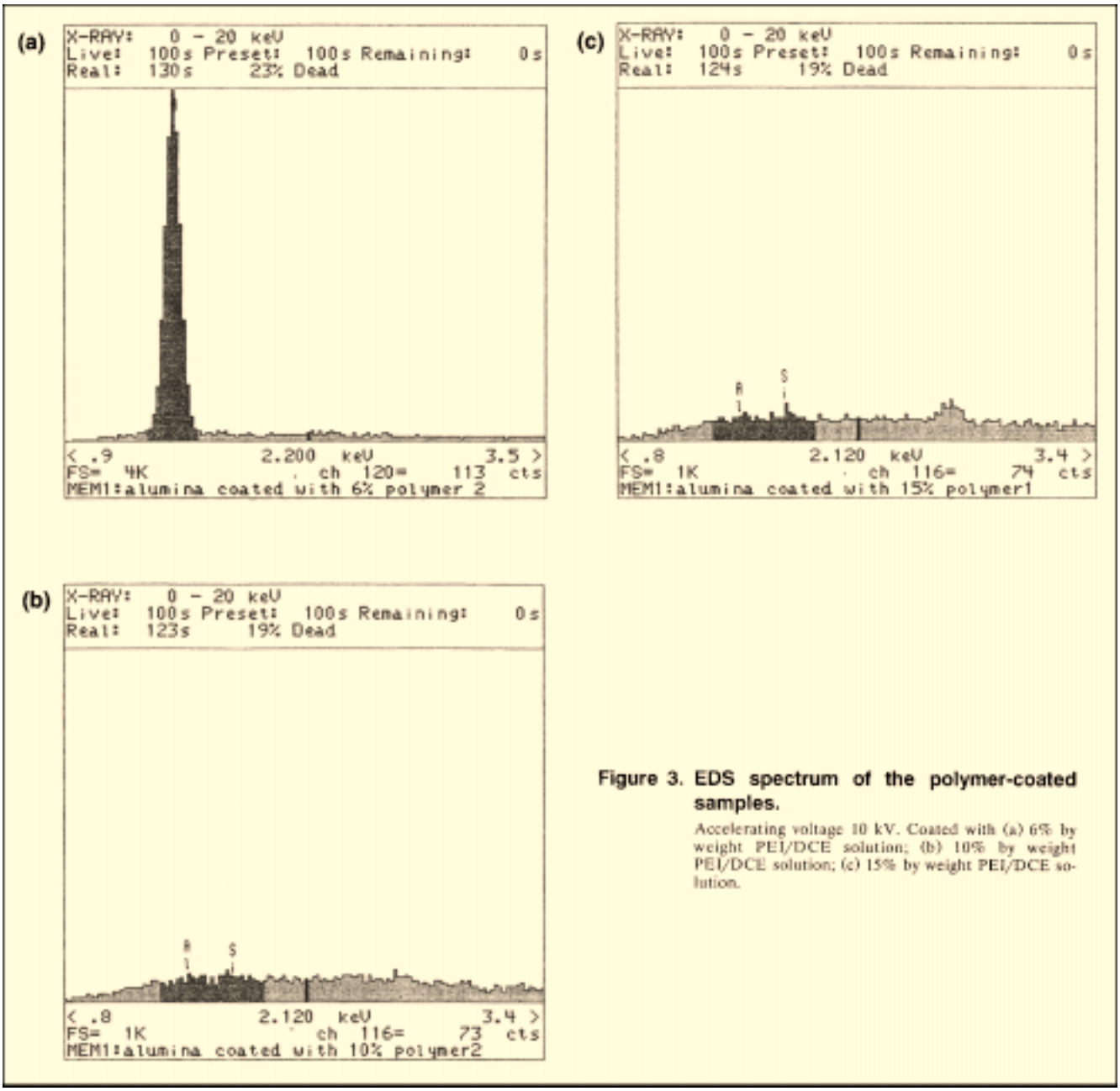

Figure 3. EDS spectrum of the polymer-coated samples.

Accelerating voltage 10 kV. Coated with (a) 6% by weight PEI/DCE solution; (b) 10% by weight PEI/DCE solution; (c) 15% by weight PEI/DCE solution.

such peaks, however, for the samples that were coated with the 10 wt. % and 15 wt. % solutions (Figures 3a and 3b). We estimate that the electron beam, generated by the 10-kV accelerating voltage, penetrates about 10^{-6} m deep. That the Al peak is completely masked, in the cases of the films created by the 10 wt. % and 15 wt. % polymeric solutions, is indicative that the film that forms on the top of the γ-alumina layer is at least 10^{-6} m thick. The very visible peak for the case of the 6 wt. % solution is indicative that the film in this case, if present at all, is significantly thinner than 10^{-6} m. Figure 4 provides the EDS spectra of the same two 10 wt. % and 15 wt. % samples taken with electron beams generated with a 20-kV accelerating voltage, for which we estimate they have penetrated roughly 2×10^{-6} m into the sample. In Figure 4a the Al peak is clearly visible, suggesting that the thickness of the polymeric film on the top of the γ-alumina layer is considerably less than 2×10^{-6} m. The Al peak size for the 15 wt. % sample is less visible, however, suggesting that the polymer film on top of the γ-alumina layer for this case is thicker than that for the 10 wt. % sample, probably about 2×10^{-6} m. These observations are also in qualitative agreement with SEM observations of the same samples, though with the latter technique it is much more difficult to pinpoint precisely where the polymer film ends and the γ-alumina/polymer layer begins. One conclusion that one draws from these studies is that it is possible to control the position and thickness of the polymer film by controlling the concentration of the polymer solution. A further detailed discussion on this issue goes beyond the scope of this article, however, and will be the subject of a future article on the topic of reproducibility in the preparation technique of CMSMs.

Figure 5 shows the cross section of the membrane after the first round of coating/carbonization. As noted previously, the image is taken without the need for gold-sputtering, since the structure is conductive by itself due to the presence of the carbon on the surface. After carbonization, at this resolution, the structure closely mimics the initial support structure, see Figure 1a (note that Figure 5 is upside down when compared to Figures 1 and 2). Carbonization appears to have loosened up the tight structure that was observed after the polymer coating (notice the difference in the α-alumina layer in Figures 5 and 2a). Figures 6a and 6b show the top γ-alumina layer after it had been coated and carbonized once (Figures 6a) and twice (Figure 6b), respectively. Comparing Figures 6a and 6b, it is obvious that the carbonized polymer clearly modifies the microstructure of the γ-alumina layer, a result that was also confirmed by gas adsorption experiments (see below). Moreover, comparing Figures 6a and 6b, it is clear that the additional coating/carbonization cycle creates a more compact and smooth layer, consistent with the observation (Sedigh et al., 1999) that the gas permeance decreases after each coating/carbonization cycle.

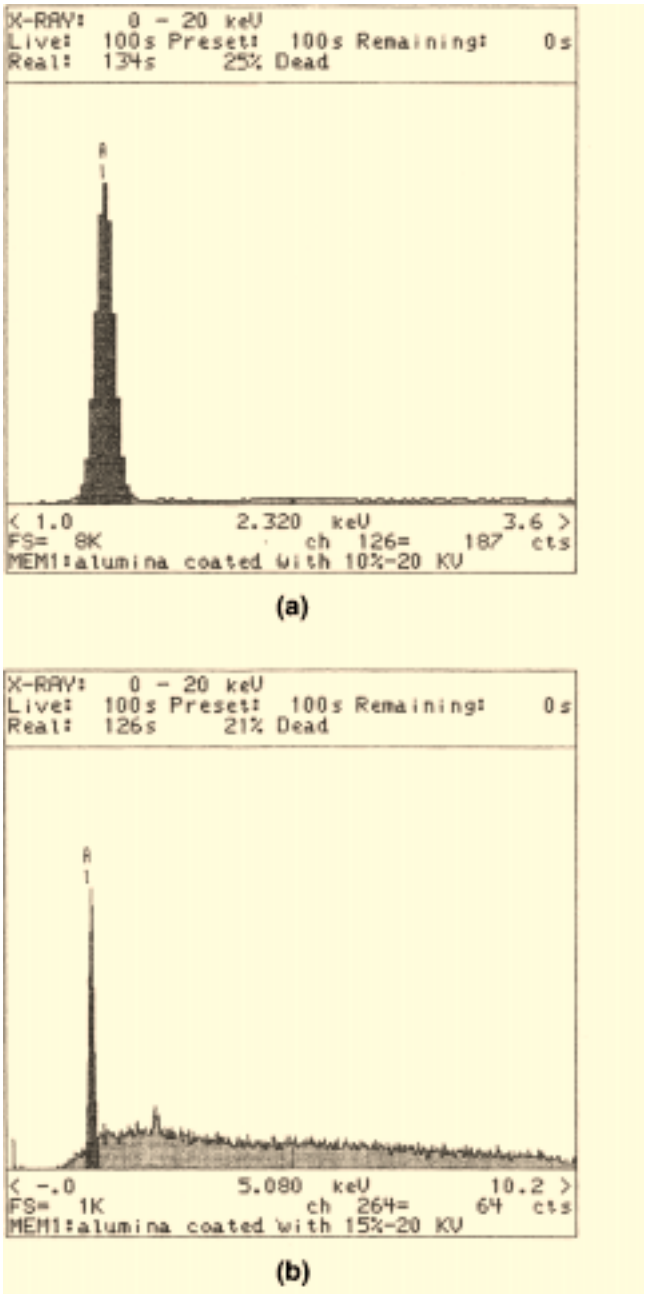

Figure 4. EDS spectrum of the polymer-coated samples.

Accelerating voltage 20 kV. Coated with (a) 10% by weight PEI/DCE solution; (b) 15% by weight PEI/DCE solution.

Gas adsorption experiments

To obtain a better picture of the microstructure of the CMSMs, and to follow the changes in their pore volume and structure as these membranes go through various preparation steps, and in order to relate these to transport and separation characteristics, we have utilized gas adsorption techniques. To establish a basis for comparison, we first studied the bare support substrates. Figure 7 represents the pore-size distribution (PSD) of the original U.S. Filter substrate, obtained by N_2 adsorption at 77 K and analyzed by the BJH method (Webb and Orr, 1998) using the desorption branch data (the adsorption isotherm is also shown in an insert in the figure, as well as in Figure 8 in order to provide a ''modeless'' picture of the adsorption characteristics during membrane synthesis). There is a peak at about 5.4×10^{-9} m, which results from the $(2-3)\times10^{-6}$-m-thick γ-alumina layer, previously referred to. It is important to note that the weight of

the γ-alumina layer, where gas adsorption mainly takes place, is a very small ($1.0-2.0\times10^{-3}$) fraction of the total weight of the support substrate. Since the weight of the γ-alumina layer was not precisely known, we opted instead to express the sorption volume in the cumulative and differential pore-volume calculations with respect to the total weight of the 0.05-m support tube. As a result, although the gas volumes measured are well above the resolution of the instrument (and therefore the resulting PSDs are highly accurate), the calculated absolute values, reported for cumulative and differential pore volumes, are rather low.

Figures 8a and 8b compare the PSD of a supported CMSM, prepared by three consecutive coating/carbonization cycles, with that of the original support substrate, both in the mesoporous (2×10^{-9} m-5×10^{-8} m) and in the microporous ($<2\times10^{-9}$ m) regions. This membrane had an ideal (ratio of single gas permeabilities) CO_2/CH_4 separation factor of about 57, with a CO_2 permeance of 3.22×10^{-7} $m^3/m^2\cdot Pa\cdot s$. The gas adsorption analysis in the microporous region was performed using N_2 at 77 K with incremental volume dosing. In the literature there are models that combine adsorption–desorption isotherms with network models of pore space and percolation theory (Sahimi, 1995). These models are usually very accurate, but are very involved and require an extensive set of data, especially for the desorption process, in order to be accurate. We do not currently have such an extensive data basis, however, and therefore the results were analyzed using the HK method, which assumes a slit-shaped pore geometry (Webb and Orr, 1998), likely to be a good assumption for the CMSM, but not so for the original substrate. As can be seen in Figure 8a, for the supported CMSM there is a sharp peak at about $(3.6-3.8)\times10^{-10}$ m, with a substantially smaller peak in the $(6-8)\times10^{-10}$-m range (the presence of peaks in the microporous region is significant; however, the absolute values for the pore sizes reported must be taken with a ''grain of salt,'' since they are much dependent on the model used for data interpretation). These values are both absent in the initial substrate. Figure 8b shows the PSD distribution of CMSMs in the mesoporous region. One can notice in this figure that the original γ-alumina layer peak has shifted from 5.4 to 3.8×10^{-9} m (the presence of the carbogenic layer also increases the amount of N_2 adsorbed). This observation is consistent with the results of the SEM studies, which show that, under this preparation protocol, the selective layer forms, mostly inside the γ-alumina layer.

In order to provide a connection between the microporous structure of the supported CMSM and the original polymeric precursor, gas adsorption experiments were carried out with powders of the pyrolyzed PEI prepared as described earlier. The pore size distribution of one such powder sample is shown in Figure 9. In this figure we include gas adsorption data using both CO_2 and N_2 as probe gases at 273 and 77 K, respectively. As can be seen, the results of both tests confirm the presence of a dominant peak at $\sim 3.7\times10^{-10}$ m. Table 1 summarizes the data of the total pore volume and BET surface area obtained by the CO_2 and N_2 adsorption experiments. The CO_2 adsorption experiment at 273 K results in both higher pore volume and surface area, because CO_2 has a higher affinity than N_2 for adsorption on carbogenic materials, and its diffusion at 273 K inside the microporous network of CMS materials is considerably faster than that of N_2 77 K. It is interesting to note, however, that both tests indicate the presence of the same peak at about 3.7×10^{-10} m.

Figure 5. SEM image of the cross section of the membrane after carbonization: 1 K magnification.

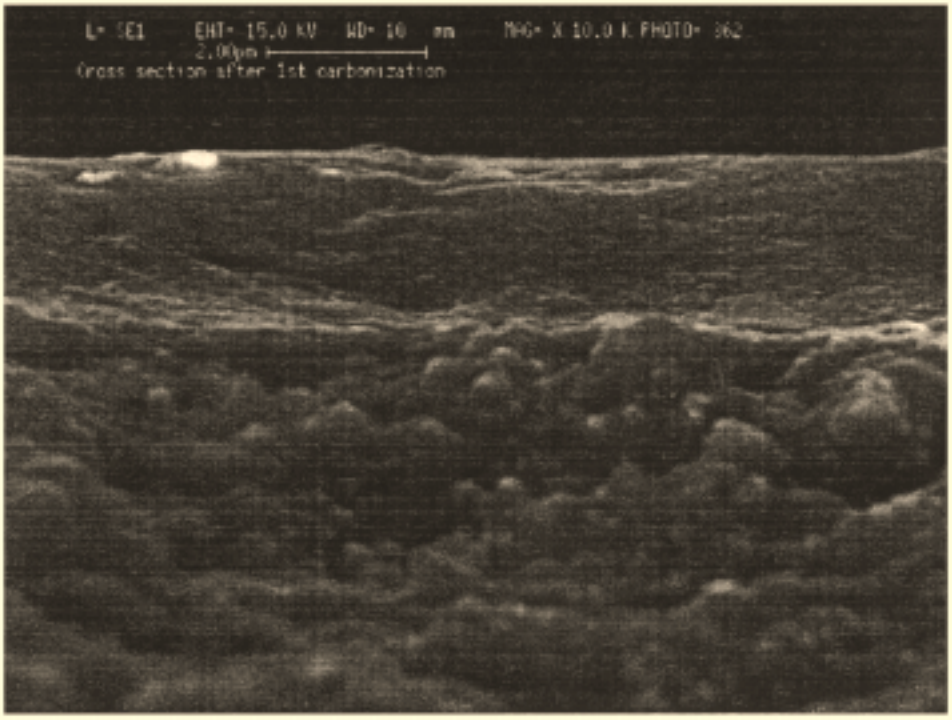

(a)

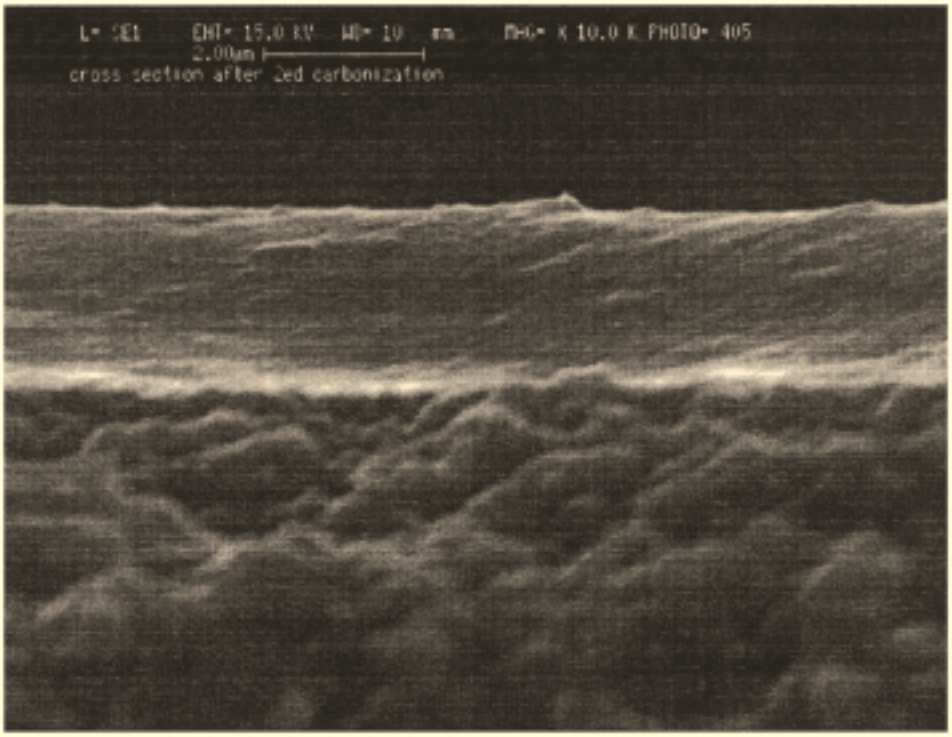

(b)

Figure 6. SEM image of the cross section, 10 K magnification: (a) after first carbonization; (b) after second carbonization.

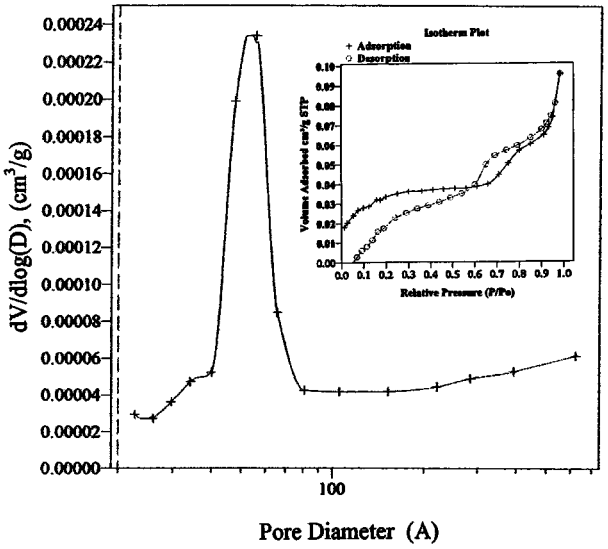

Figure 7. Pore-size distribution and adsorption isotherm of support substrate.

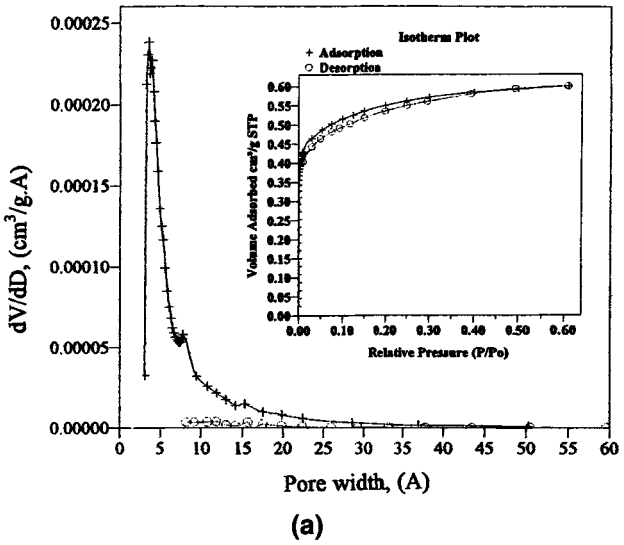

(a)

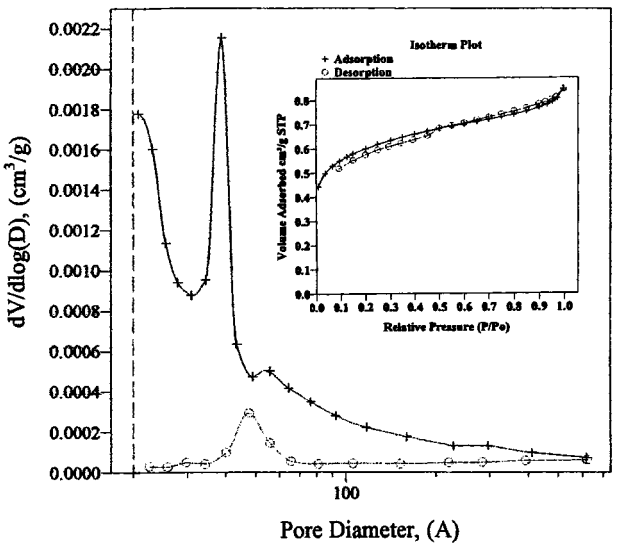

(b)

Figure 8. PSD and adsorption isotherm of the CMSM and PSD of support substrate (+ CMSM, ○ support substrate): (a) microporous region; (b) mesoporous region.

In addition, the N_2 adsorption analysis at 77 K also revealed the presence of a smaller shoulder peak (as previously noted, due to experimental limitations, in our system about, 6×10^{-10} m is the upper limit of application for the CO_2 adsorption experiments, and as a result a similar peak could not be detected using CO_2 at 273 K). A similar shoulder peak was also previously observed with the supported CMSM, though for the powders this peak is shifted to about 10^{-9} m.

We have also used gas adsorption experiments to study the effect that each additional cycle of coating/carbonization has on the microstructure of the resulting membranes. The results for two cycles of coating/carbonization for one of the supported membranes that were prepared are shown in Figure 10. Table 2 summarizes the transport characteristics in terms of the single gas permeance and separation factor for the same membrane after each coating/carbonization step. The CO_2/CH_4 ideal separation factor increased from 1.5 to 12.5 as the CO_2 permeance decreased by about 50% in value. By comparing the adsorption data in Figure 10 in the region of pore diameters under 6×10^{-10} m, the conclusion is that there is little difference between the first and second coating/carbonization cycles. After the second coating/carbonization cycle the primary microporous peak remains unchanged, while there is a slight decrease in the peak's pore volume from 1,750 to 1,600 $m^3/kg\cdot m$. However, there is a difference between the PSD after the first and second cycles, in that there is a reduction of the pore volume of the pores bigger than 6×10^{-10} m, extending all the way to the mesoporous region. In our opinion, this explains the increase in separation factor from 1.5 to 12.5 and also the lowering of the permeance.

The direct relationship that exists between the membrane's microstructure and its transport characteristics was also studied for the membrane of Figure 8 after its transport characteristics had been degraded due to prolonged exposure to heavy oil vapors. Table 3 summarizes the separation factor and CO_2 permeance of this membrane in its original state and after it had degraded. Table 3 shows both the separation factor and the CO_2 permeance of the membrane decreased as a result of degradation of the membrane. Upon the completion of the transport experiments it was theorized that this is likely to be the result of micropore volume clogging, that is, of the selective pores of the membrane with an average width of about $(3.6–3.8)\times10^{-10}$ m, due to the adsorption of organic vapors. This view is consistent with N_2 adsorption data for both the fresh membrane and the membrane that had been degraded, which are shown in Figure 11. Note the significant reduction of the N_2 adsorption peak in the (3.6–3.8) $\times10^{-10}$-m region for the degraded membrane as compared with the original fresh membrane. One also concludes that, to have undergone the evacuation of the sample in the micro-

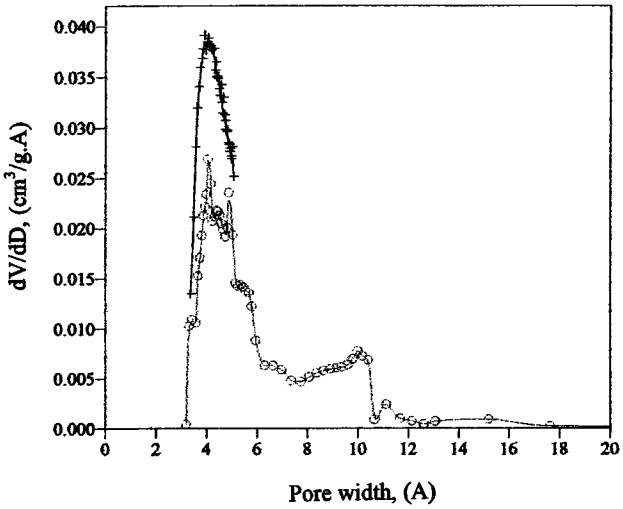

Figure 9. PSD of the pyrolyzed PEI at 873 K. (+ CO_2 adsorption, ○ N_2 adsorption).

Table 1. Results of Adsorption Experiments

	CO_2	N_2
Pore volume (m^3/kg)	1.01×10^{-4}	8.2×10^{-5}
BET surface (m^2/kg)	2.45×10^{5}	1.573×10^{5}

pore analyzer without being desorbed, whatever has clogged this micropore region is strongly held there. It should be clear from the preceding discussion that there is a close tie between the micro-/mesostructure of the CMSM and its transport and separation characteristics. Pore-size distribution and pore volume are a significant indicator of membrane performance in terms of its ability to separate gaseous species, which are slightly different in their molecular kinetic diameters.

Conclusions

Supported PEI-based CMSMs were studied in an attempt to relate their transport properties to their structural characteristics. A number of structural characterization experiments were performed with the CMSMs, the support substrates, as well as with the pyrolyzed PEI powder. SEM and EDS analyses were utilized in order to identify the position of the polymeric precursor film and of the final carbon layer within the support's pore structure. Where the carbon layer is located depends on the concentration of the initial polymeric precursor and on the rest of the dip-coating conditions.

To confirm the SEM observations, and in order to relate the membrane's transport and separation characteristics to its microstructure, micropore volume analysis using the gas adsorption technique was also performed. N_2 adsorption in the microporous region revealed the presence of a sharp peak at about $(3.6–3.8)\times10^{-10}$ m. This peak is absent in the original support substrate. These are the pores which, in our opinion, are responsible for the molecular sieving properties of the supported CMSM. Micropore analysis of pyrolyzed PEI powders has shown a similar peak, indicating that this peak is

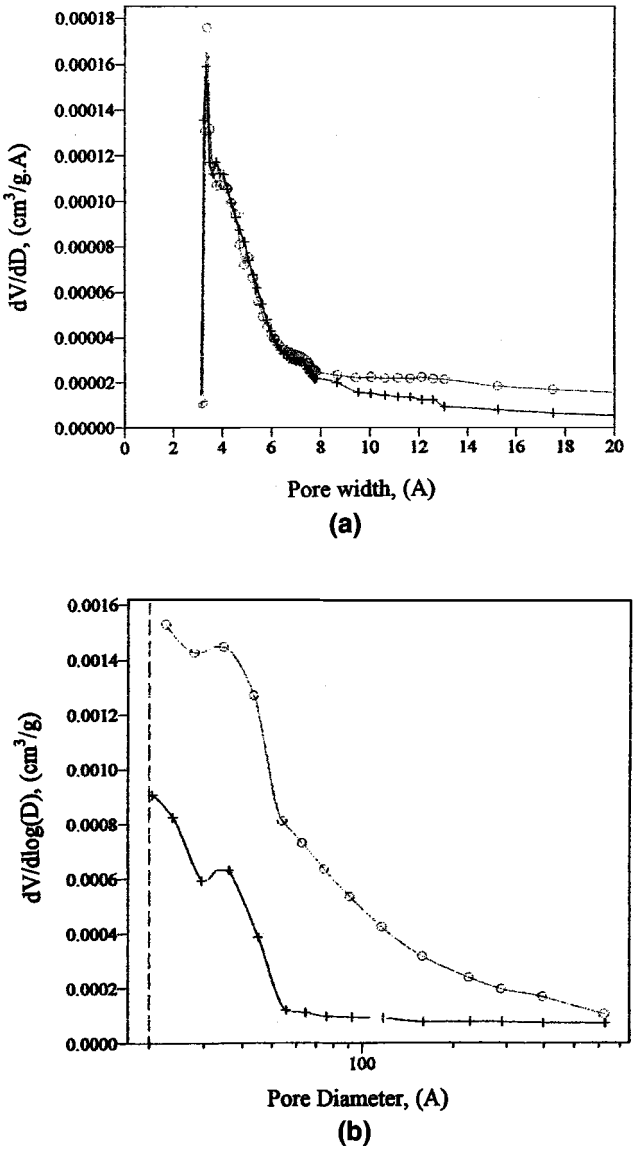

Figure 10. PSD of CMSM after first and second carbonization, (○—first carbonization, +—second carbonization): (a) microporous region, (b) mesoporous region.

Table 2. Transport Characteristics

	1st Carbonization	2nd Carbonization
CO_2 permeance	2.4505×10^{-6}	1.149×10^{-6}
CO_2/CH_4 sep. fac.	1.5	12.5

Permeance: $m^3/m^2\cdot Pa\cdot s$.

Table 3. Membrane Decrease Due to Its Degradation

	Original Membrane	After Degradation
CO_2 permeance	3.202×10^{-7}	3.829×10^{-8}
CO_2/CH_4 sep. fac.	57	4.4

Permeance: $m^3/m^2\cdot Pa\cdot s$.

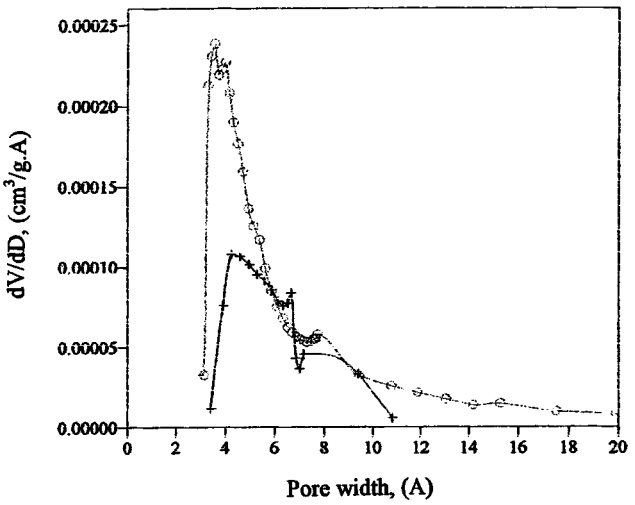

Figure 11. PSD of original CMSM (○), and degraded membrane (+) in the microporous region.

an intrinsic characteristic of the pyrolyzed polymer. It was also observed that after each coating/carbonization step, while the magnitude of the $(3.6–3.8)\times10^{-10}$-m peak only slightly changed, there was a considerable reduction in the pore volume in the tail of the PSD curve in the micro- and mesoporous regions, which in our opinion indicates a reduction in the number of micro- and mesoscopic size cracks and pinholes. This is probably one of the main reasons for obtaining higher separation factors and lower permeances after each additional coating/carbonization cycle. The study of a membrane, whose properties had degraded (due to exposure to organic vapors), provided similar clues. It was observed, for example, that after the membrane had degraded, the pore volume in the $(3.6–6)\times10^{-10}$-m range drastically decreased, and both the separation factor and permeance of the membrane simultaneously decreased. The reduction of the pore volume was mainly attributed to the adsorption of large organic compounds.

Acknowledgment

We are grateful to the National Science Foundation and the U.S. Department of Energy for partial support of this study.

Literature Cited

Acharya, M., B. A. Raich, H. C. Foley, M. P. Harold, and J. J. Lerou, "Metal Supported Carbogenic Molecular Sieve Membranes: Synthesis and Applications," *Ind. Eng. Chem. Res.*, **36**, 2924 (1997).

Chen, Y. D., and R. T. Yang, "Preparation of Carbon Molecular Sieve Membrane and Diffusion of Binary Mixtures in the Membrane," *Ind. Eng. Chem. Res.*, **33**, 3146 (1994).

Economy, J., M. Daley, E. J. Hippo, and D. Tandon, "Elucidating the Pore Structure of Activated Carbon Fibers through Direct Imaging using Scanning Tunneling Microscopy (STM)," *Carbon*, **33**, 344 (1995).

Ehrburger, P., N. Pusset, and P. Dziedzinl, "Active Surface Area of Microporous Carbons," *Carbon*, **30**, 1105 (1992).

Hayashi, J., M. Yamamoto, K. Kusakabe, and S. Morooka, "Simultaneous Improvement of Permeance and Permselectivity of 3,3′,4,4′-Biphoenyltetracarboxylic-Dianhydride-4,4′-Oxydianiline Polyimide Membrane by Carbonization," *Ind. Eng. Chem. Res.*, **34**, 4364 (1995).

Hayashi, J., H. Mizuta, M. Yamamoto, K. Kusakabe, S. Morooka, and S. Sush, "Separation of Ethane/Ethylene and Propane/Propylene Systems with a Carbonized BPDA-PP′ ODA Polyimide Membrane," *Ind. Eng. Chem. Res.*, **35**, 4176 (1996).

Hayashi, J., H. Mizuta, M. K. Yamamoto, K. Usakabe, and S. Morooka, "Pore Size Control of Carbonized BPDA-PP′ ODA Polyimide Membrane by Chemical Vapor Deposition of Carbon," *J. Memb. Sci.*, **124**, 243 (1997).

Hoffman, W. P., M. B. Fernandez, and M. B. Rao, "Characterization of Porosity in Nanoporous Carbons Using Scanning Tunneling Microscopy," *Carbon*, **32**, 1383 (1994).

Inagaki, M., and M. Nakashima, "Irreversible Adsorption of Carbon Dioxode Gas on an Activated Carbon," *Carbon*, **30**, 1135 (1992).

Jagiello, J., T. J. Bandosz, K. Putyera, and J. A. Shwarz, "Micropore Structure of Template—Derived Carbons Studied Using Adsorption of Gases with Different Molecular Diameters," *J. Chem. Soc. Faraday Trans.*, **91**, 2929 (1995).

Koresh, J. E., "New Molecular Probe Technique for the Assessment of Ultramicroporous Structure," *J. Chem. Soc. Faraday Trans.*, **89**, 2059 (1993).

Kumita, M., J. Ozaki, J. Kobayashi, M. Ito, F. Watanda, and M. Hasatani, "Characteristics of Helium Adsorption on Microporous Solids Under Cryogenic Conditions," *J. Chem. Eng. Jpn.*, **28**, 159 (1995).

Linkov, V. M., R. D. Sanderson, and E. P. Jacobs, "Highly Asymmetrical Carbon Membranes," *J. Memb. Sci.*, **95**, 93 (1994a).

Linkov, V. M., R. D. Sanderson, and E. P. Jacobs, "Carbon Membranes from Precursors Containing Low-Carbon Residual Polymers," *Polymer Inter.*, **35**, 239 (1994b).

Miura, K., J. Hayashi, T. Kawaguchi, and K. Hashimoto, "A Shape-Selective Catalyst Utilizing a Molecular Sieving Carbon with Shape Pore Distribution," *Carbon*, **31**, 667 (1993).

Nakashima, M., S. Shimada, M. Inagaki, and T. A. Centeno, "On the Adsorption of CO_2 by Molecular Sieve Carbons: Volumetric and Gravimetric Studies," *Carbon*, **33**, 1301 (1995).

Rao, M. B., and S. Sircar, "Nanoporous Carbon Membranes for Separation of Gas Mixtures by Selective Surface Flow," *J. Memb. Sci.*, **85**, 253 (1993).

Rao, M. B., and S. Sircar, "Performance and Pore Characterization of Nanoporous Carbon Membranes for Gas Separation," *J. Memb. Sci.*, **110**, 109 (1996).

Sahimi, M., *Flow and Transport in Porous Media and Fractured Rock*, Chap. 5, VCH, Weinheim, Germany (1995).

Sedigh, M. G., W. J. Onstot, L. Xu, W. L. Peng, T. T. Tsotsis, and M. Sahimi, "Experiments and Simulation of Transport and Separation of Gas Mixtures in Carbon Molecular Sieve Membranes," *J. Phys. Chem. A*, **102**, 8580 (1998).

Sedigh, M. G., L. Xu, T. T. Tsotsis, and M. Sahimi, "Transport and Morphological Characteristics of Polyetherimide-Based Carbon Molecular Sieve Membranes," *Ind. Eng. Chem. Res.*, **38**, 3367 (1999).

Setoyama, N., K. Kaneko, and F. Rodriguez-Reinoso, "Ultramicropore Characterization of Microporous Carbon by Low Temperature Helium Adsorption," *J. Phys. Chem.*, **100**, 10331 (1996).

Steriotis, T., A. Beltsios, C. Mitropoulos, W. Kanellopoulos, S. Tennison, A. Wiedeman, and V. Keiderling, "On the Structure of an Asymmetric Carbon Membrane with a Novolax Resin Precursor," *J. Appl. Poly. Sci.*, **64**, 2323 (1997).

Webb, P. A., and C. Orr, *Analytical Methods in Fine Particle Technology*, Micromeritics Instrument Corporation, Norcross, GA (1998).

Yoshizawa, W., M. Yamada, M. Shiraishi, K. Kaneko, and N. Setryama, "Evaluation of Accessible and Inaccessible Microporosities of Microporous Carbons," *J. Chem. Soc. Faraday Trans.*, **92**, 2297 (1996).

Manuscript received Feb. 15, 2000, and revision received May 30, 2000.